On the role of the seawater absorption to attenuation ratio in the radiance polarization above the Southern Baltic surface

Włodzimierz Freda[1], Kamila Haule[1], Sławomir Sagan[2]

[1]Department of Physics, Gdynia Maritime University, Gdynia, 81-225, Poland
[2]Institute of Oceanology, Polish Academy of Sciences, Sopot, 81-712, Poland

Correspondence to: Włodzimierz Freda (wfreda@am.gdynia.pl)

Abstract. Information about polarization of light leaving the ocean surface has the potential to improve the quality of the bio-optical parameters retrieval from ocean color remote sensing (OCRS). This improvement can be applied in numerous ways such as limiting of sun glints and obtaining information about atmospheric aerosol properties for atmospheric correction as well as increasing the accuracy of the algorithms based on the water-leaving signal. Polarization signals at the top of the atmosphere (ToA) that include the water-leaving signal are strongly influenced by atmospheric molecular scattering and by direct sun and sky reflections from the sea surface. For these reasons, it is necessary to better understand the factors that change the polarization of light in the atmosphere-ocean system, especially in coastal zones affected by dynamic changes. In this paper, the influence of seasonal variability of light absorption and scattering coefficients (inherent optical properties, IOPs) of seawater, wind speed and solar zenith angle (SZA) on the polarization of upwelling radiance over the sea surface in the visible light bands is discussed. The results come from a polarized radiative transfer model based on the Monte Carlo code and applied to the atmosphere-ocean system using averaged IOPs as input data. The results, presented in the form of polar plots of the total upwelling radiance degree of polarization (DoP), indicate that regardless of the wavelength of light and type of water, the highest value of the above water DoP is strongly correlated with the absorption-to-attenuation ratio. The correlation is a power function that depends on both the SZA and the wind speed. The correlation versatility for different wavelengths of light is very unusual in optics of the sea and is therefore worth emphasizing.

1 Introduction

Satellite ocean color radiometry has been developed for decades to study the interaction of a light field within the visible part of the spectrum (i.e., 400-700 nm) with the different optically significant constituents of sea water. The research has been focusing on information coming from the intensity of water-leaving light - its measurement, retrieval, correlations and interpretation (e.g., Volpe et al., 2012; Zibordi et al., 2013; Sammartino et al., 2015). However, in addition to the light intensity, consideration of light polarization has been demonstrated to improve the accuracy of the information from a variety of remote sensing applications, i.e., in remote radar measurements (Hajnsek et al., 2003; Soloviev et al., 2012;

1

Benassai et al., 2013), in atmospheric correction algorithms (Chowdhary et al., 2002), in above-surface measurements (Garaba and Zielinski, 2013) and in beneath-surface measurements (Ibrahim et al., 2012).

Theoretical and field measurements have shown that the polarization of the underwater light field is sensitive to the nature of the suspended marine particles. Ibrahim et al. (2012) demonstrated that the attenuation-to-absorption ratio influences the polarization of upwelling radiance below the sea surface. Polarized measurements have also been performed near and above the sea surface. Reduction of sun glints to improve the ocean color retrieval has been studied by Zhou et al. (2017) as well as Garaba and Zielinski (2013) and limitation of sky reflections by observation of sea surface at the Brewster angle from the ship board has been examined by Wood and Cunningham (2001) and by Cunningham et al. (2002). Polarization distribution of skylight reflected off the rough sea surface has been examined by Zhou et al. (2013). They simulated the degree of polarization as well as the angle of polarization (AoP) for reflected parts of upwelling radiance and discussed its variability with SZA for 0°, 30°, 60° and 90°. Moreover, Zhou et al. (2013) showed the influence of wind speed and direction on the polarization pattern of reflected radiance. Radiative transfer simulations have shown the effect of marine suspensions on the polarization of light recorded above the sea surface (see Chami et al.,2005; Chami, 2007). Further studies have also shown the possibility of knowing the composition of the suspension, i.e., the ratio of mineral to organic suspension, using polarization properties of water-leaving radiance (see Gilerson et al., 2006; Chami, 2007; Tonizzo et al., 2011). The intent of the authors was to show the seasonal variability of polarization of the upwelling radiance above the sea surface.

The most challenging part in the analysis of the signal registered by passive radiometric sensors at the top of the atmosphere is to remove the contribution of the reflected photons at the air-sea interface as well as the contribution of the atmosphere. To assess the water-leaving radiance, $L_w(\lambda)$ on the level of accuracy required to derive accurate estimates of the desired water components, other characteristics and methods that support the advanced atmospheric correction and parameter retrieval have been searched, i.e., the black pixel assumption (Siegel et al., 2000), using near infrared and shortwave infrared bands (Wang et al., 2007), using unpolarized ToA reflectance (Frouin et al., 1994), or using polarized water-leaving radiance (Zhai et al. 2017). The latter showed that, in general, the polarized signal at the ToA is 2-3 times higher than its water-leaving part because of the influence of molecular scattering in the atmosphere. Discussions on the use of remote polarization measurements to determine the aerosol properties that can then be used for atmospheric correction are included in Chowdhary et al. (2002), Mishchenko and Travis (1997) as well as Hasekamp and Landgraf (2005). Pust et al. (2011) showed that measurements of the degree of polarization of the sky (made from the ground) can also be helpful in obtaining aerosol parameters. He et al. (2014) proposed to measure the parallel polarization radiance (PPR) instead of radiance intensity at ToA. According to them, such measurements would enhance the OCRS capability. Liu et al. (2017), based on radiative transfer modeling and laboratory measurement, showed that the concentration of particulate matter influences the PPR measured at ToA.

Polarized signal can be measured from the satellite sensors, e.g., POLarization and Directionality of the Earth's Reflectances sensor (POLDER-2), above water using a polarization imaging camera (Freda et al., 2015) or underwater as by Loisel et al. (2008) and Harmel et al. (2008). The measurements are often supported by numerical modeling. Although there are many

ongoing numerical radiative transfer models, very few of them include light polarization (Piskozub and Freda, 2013; Chami et al., 2001). Most current methods of radiative transfer treat light as a scalar to hasten the computations. Polarized radiative transfer was first applied by Chami et al. (2001) to retrieve the polarizing properties of the marine phytoplankton and minerals for different water conditions. Their analysis revealed that the application of the polarization of light in ocean color

5   algorithms might significantly improve the retrieval of hydrosol properties, especially in coastal waters. Piskozub and Freda (2013) applied their polarized radiative transfer model to the Baltic Sea. They examined how scattering properties of seawater represented by a single scattering albedo affected the polarization of water-leaving radiance. They demonstrated the impact of air bubble layers of various concentrations on the degree of polarization of water-leaving light. They also concluded that polarization remote sensing should be performed on a plane tilted approximately 90° from the solar azimuth

10   angle to avoid sun glints.

The involvement of polarization in radiative transfer analysis seems to be especially important in coastal areas, knowing that they undergo dynamic changes due to human proximity (Drozdowska et al., 2017), river inflows and the occurrence of pollution, including optically significant oil pollution (Drozdowska et al., 2013). Nevertheless, little attention has been paid to the measurement and modeling of light polarization in coastal areas and closed water basins characterized by optically

15   complex waters. The Baltic Sea represents a region of a great economic importance, extremely high marine traffic and the impact of inflows from nine different surrounding countries. Inherent optical properties of Baltic seawater and its constituents have been in the spotlight for oceanographers for two decades. In addition to regular measurements of depth profiles of absorption and attenuation coefficients, measurements for different components of seawater have been performed. Colored dissolved organic matter (CDOM) is known to be the primary absorber in the Baltic Sea (Kowalczuk et al., 2010),

20   and its impact on the total absorption coefficient for blue light can reach up to 80% (Kowalczuk et al., 2005). Kowalczuk (1999) and Kowalczuk and Kaczmarek (1996) found that the high absorption of CDOM in spring and low absorption in winter is due to the biological cycle as well as the seasonal variability of the inlet with river water and its mixing. The search for a better correlation of the spectral remote sensing reflectance R_{rs} ratio with the absorption coefficient of CDOM has been intensively searched within the SatBaltic system (Meler et al., 2016a). Measurements of suspended matter IOPs in the Baltic,

25   i.e., particle absorption and particle scattering coefficients, have been compared with biogeochemical characteristics of suspended matter such as concentrations of suspended particulate matter, particulate organic matter, particulate organic carbon and chlorophyll a (Woźniak et al., 2011). Meler et al. (2016b) concluded that absorption properties of non-algal particles undergo larger regional than seasonal variability. In addition to the absorption and attenuation coefficients, the volume scattering functions (VSFs) were also measured in the waters of the Southern Baltic (Freda et al., 2007; Freda and

30   Piskozub, 2007; Freda, 2012). Unique measurements have been performed by the prototype volume scattering meter, characterized by an angular resolution of 0.3º and a range of scattering angles from 0.6º to 177.9º, described by Lee and Lewis (2003). The same instrument has also been used by Chami et al. (2005) in the Black Sea and by Berthon et al. (2007) in the Adriatic Sea. Baltic Sea waters are often affected by small-scale oil pollution (Rudź et al., 2013). The influence of dispersed oil droplets on the absorption coefficient of seawater was researched by Otremba (2007) as well as Haule and

Freda (2016), while their influence on scattering properties has been tested by Freda (2014). The consequences of changes in IOPs for remote detection of dispersed oil pollution have been discussed by Otremba et al. (2013), Otremba (2016), and Haule et al. (2017) based on radiative transfer modeling. Knowledge and datasets collected in the Baltic throughout the past two decades helped us to perform a unique study on polarized radiation above the southern Baltic sea surface. This study

5   shows the application of a polarized radiative transfer model in three optically different regions, two seasons and two different sea states. The study highlights the possibilities and consequences of including polarization information in bio-optical models of seawater.

2 Methods

The difficulty of comparison of upwelling radiance DoP over a wind-roughened southern Baltic surface for various seasons

10   is caused by the small number of sunny days in winter and too many variable weather factors that would make it difficult to explain the differences. These undesirable weather factors are different aerosol optical depths, sky overcast, and changing speed and direction of wind relative to the position of the sun. For those reasons, we applied a polarized radiative transfer model based on the Monte Carlo code to describe the effect of seasonal changes on the polarization of upwelling radiance. The simulations involved seasonally averaged measurements of inherent optical properties from the Southern Baltic basin

15   and were run for constant weather conditions. For a detailed description of the inputs and conditions under which the simulation is performed, see the following subsections.

2.1 Polarized radiative transfer model - theoretical background

Numerical simulations were carried out using the Monte Carlo algorithm created by Jacek Piskozub and described in Piskozub and Freda (2013). The algorithm solves the vector radiative transfer equation for the atmosphere-ocean system

20   using the successive orders of scattering method and the Stokes formalism to track the polarization of photons. The algorithm collects information about virtual photons involved statistically in optical processes: reflection at the rough sea surface, refraction at the air-water interface, scattering and absorption within the water body and reaching the ToA. Moreover, the algorithm tracks polarization changes of each photon during these processes. Polarization information is described by four elements of the Stokes vector: $S = [I,Q,U,V]^T$, where I is the total radiance of light, Q describes the

25   radiance of linearly polarized light (vertical to horizontal), U describes the radiance of linearly polarized light (diagonal right-skewed to left-skewed), V describes the circular polarization (clockwise to counterclockwise) and T denotes the transposition. Three elements (Q, U and V) of the Stokes vector may be both positive or negative. The single quantity that characterizes these properties is the degree of polarization:

$$DoP = \frac{\sqrt{Q^2+U^2+V^2}}{I}, \tag{1}$$

30   The defined degree of polarization is often replaced by the degree of linear polarization, DoLP.

$$DoLP = \frac{\sqrt{Q^2+U^2}}{I},$$ (2)

The latter hardly differs from DoP because circular polarization represented by the V element of the Stokes vector is negligible in sea water (see off-diagonal Mueller matrix elements in (Voss and Fry, 1984)).

Our polarized radiative transfer model involves a virtual light source to send randomly polarized photons and track their
5   pathways in the means of the probability of occurrence of the processes mentioned above. Reflection and refraction processes are basically described by Fresnel equations, and the slopes of the sea surface are characterized by the wind-dependent distribution of Cox and Munk (1956). The probability of processes within the water body is determined by the corresponding coefficients of absorption and scattering (including multiple scattering). Angular distribution of scattered photons is described by phase functions that, for both atmosphere and sea depth, are characterized separately for molecular
10   scattering and particle scattering. Polarization properties of particle scattering are described by Müeller matrices that for sea water are taken from Voss and Fry (1984) and for atmospheric aerosol particles from Volten et al. (2001). The Müeller matrix and thus the total and polarized phase function of the particles is computed by means of Mie theory. The model outputs the angular distribution of the upwelling radiance and its degree of polarization at any desired level. All results are specified in the principal plane.

15   **2.2 Polarized radiative transfer model - input parameters**

This section reports the input parameters used in the computations. The data set of the absorption and attenuation coefficients of seawater constituents come from *in situ* measurements in the southern Baltic contained in Sagan (2008). It is the largest dataset of ac-9 measurements in the southern Baltic that was published in a tabular form of average values, extreme values and standard deviations. The instrument was calibrated in ultrapure water and routinely checked for stability
20   with air readings. The standard recommended data processing was performed (Zaneveld et al. 1994). Absolute precision of measurement is 0.005 m^{-1}, while relative precision is estimated from 4% in clear waters to 12% in the areas of turbid waters. The data have been recorded during cyclical cruises aboard R/V Oceania in 1999 and 2003 to 2005. Measurements were made in different months of the year. The data set was divided into two seasons, called here 'winter', for the months from November to March and 'summer', the months from April to October. The summer season is characterized by strong
25   phytoplankton growth and the winter season by low biological activity. In addition, Sagan (2008) distinguished three regions: open Baltic, gulfs (Gulf of Gdańsk and Pomeranian Gulf) and coastal waters. The measuring stations, divided into these three types of water, are shown in Figure 1. For defined regions – open Baltic and coastal areas – those two data sets are statistically significantly different for all optical parameters (*t* test for means) at the level p<0.05 by Sagan (2008).

Total absorption coefficient taken to the simulation is a sum $a = (a - a_w) + a_w$, where $(a - a_w)$ is an average absorption
30   coefficient of the N number of measured depth profiles (see Table 1) made with the ac-9 after Sagan (2008), and a_w is the pure water absorption coefficient and comes from Pope and Fry (1997). Similarly, the total attenuation coefficient is defined

Ocean Science
Discussions

Open Access

EGU

as $c = (c - c_w) + a_w + b_w$, where the component $(c - c_w)$ comes directly from Sagan (2008), but to get the total attenuation coefficient, it was enlarged by clean water components of absorption a_w and scattering b_w (Smith and Baker, 1981). According to Sagan (2008), the highest values of IOPs and their highest variability are observed for the water of gulfs and estuaries of rivers that are located nearby. The simulations are carried out at nine wavelengths, namely, 412 nm, 440 nm, 488

5   nm, 510 nm, 532 nm, 555 nm, 650 nm, 676 nm and 715 nm, which correspond to the ac-9 and are commonly dedicated to ocean color analysis.

Solar zenith angles in the southern Baltic region depend strongly on the season. In months described by Sagan (2008) as the summer season, the highest sun position over the horizon, that means the minimum of SZA during sun culmination, varies between 31º in June (the longest day of the year) and 69º at the end of October. In the modeling, a single value of 45º was

10   chosen as a summer SZA. For months of the winter season, the minimum of SZA varies between 50º in the end of March and 78º in December (the shortest day). Given values are reached at approximately noon and are higher in the rest of the days. That is why SZA of 75º is chosen as a representative for the winter season. Computations are performed for the direction of wind twisted by 45º from the sun reflection plane, chosen arbitrarily. Two wind speeds of 5 m/s and 15 m/s are considered.

15   Here and in the following figures, the celestial hemisphere and its reflection patterns are represented in a two-dimensional coordinate system. The zenith and the nadir are at the origin and the horizon is represented by the outermost circle. The zenith angle and azimuth angle are measured radially and tangentially, respectively. The solar azimuth angle is always set to 0.
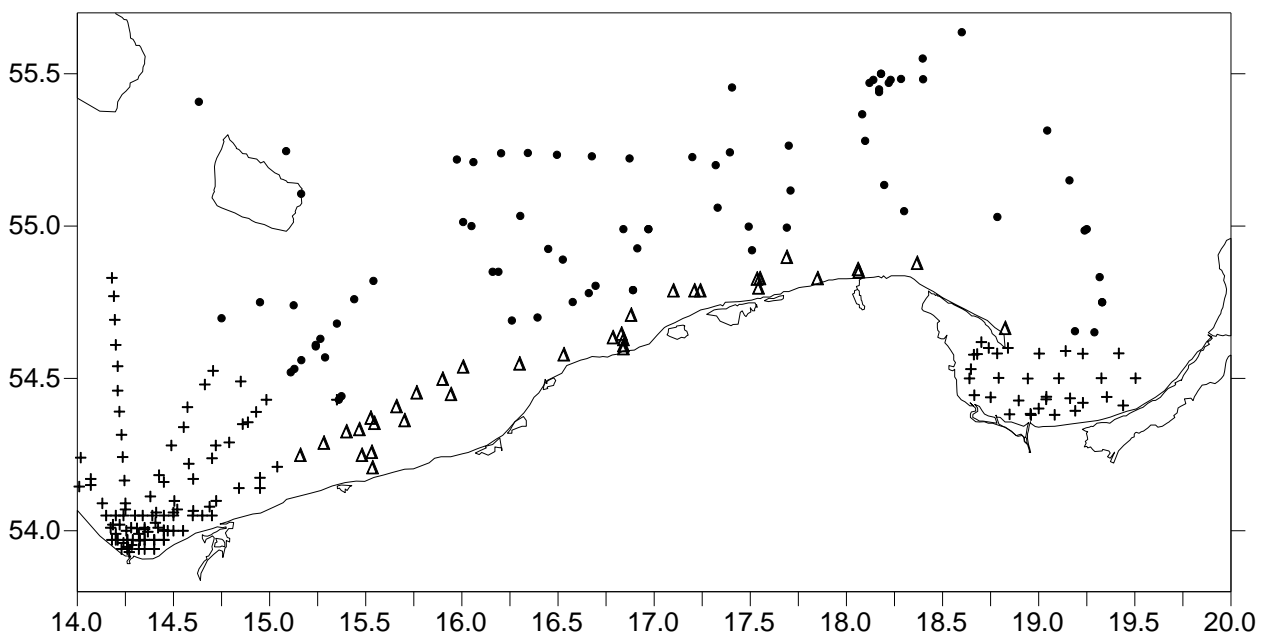
20   **Figure 1. The area of the southern Baltic Sea, on which the positions of measurement stations are marked, divided into three areas: Pomeranian Gulf and Gulf of Gdańsk (+), coastal water (Δ) and open Baltic water (•).**

Table 1. Average values of total absorption coefficients, total attenuation coefficients, their standard deviations and their ratios. All values measured by Sagan (2008) in southern Baltic in 1999 and 2003 to 2005 are averaged for depths 0 to 5 meters and then averaged for N measuring stations

| λ	Baltic, N=930					Gulfs, N = 1428					Coastal Waters, N = 132				
						Summer Season									
[nm]	$a(\lambda)$	σ_a	$c(\lambda)$	σ_c	$\frac{a(\lambda)}{c(\lambda)}$	$a(\lambda)$	σ_a	$c(\lambda)$	σ_c	$\frac{a(\lambda)}{c(\lambda)}$	$a(\lambda)$	σ_a	$c(\lambda)$	σ_c	$\frac{a(\lambda)}{c(\lambda)}$
412	0.595	0.12	1.230	0.40	0.483	1.095	0.65	2.560	1.64	0.428	0.615	0.12	1.470	0.52	0.418
440	0.396	0.10	0.999	0.37	0.396	0.786	0.52	2.209	1.48	0.356	0.416	0.10	1.249	0.52	0.333
488	0.214	0.07	0.817	0.34	0.262	0.444	0.32	1.887	1.35	0.236	0.214	0.06	1.027	0.46	0.209
510	0.183	0.05	0.785	0.33	0.233	0.353	0.23	1.825	1.31	0.193	0.173	0.04	0.995	0.46	0.173
532	0.155	0.04	0.756	0.32	0.205	0.285	0.18	1.756	1.28	0.162	0.155	0.03	0.946	0.44	0.163
555	0.140	0.03	0.731	0.31	0.192	0.240	0.13	1.711	1.26	0.140	0.140	0.03	0.911	0.42	0.153
650	0.380	0.02	0.921	0.29	0.413	0.430	0.08	1.811	1.20	0.237	0.380	0.02	1.071	0.38	0.355
676	0.518	0.05	1.029	0.28	0.503	0.638	0.19	1.909	1.18	0.334	0.508	0.03	1.169	0.38	0.435
						Winter Season									
λ	Baltic, N = 234					Gulfs, N = 540					Coastal Waters, N = 36				
[nm]	$a(\lambda)$	σ_a	$c(\lambda)$	σ_c	$\frac{a(\lambda)}{c(\lambda)}$	$a(\lambda)$	σ_a	$c(\lambda)$	σ_c	$\frac{a(\lambda)}{c(\lambda)}$	$a(\lambda)$	σ_a	$c(\lambda)$	σ_c	$\frac{a(\lambda)}{c(\lambda)}$
412	0.485	0.03	0.680	0.015	0.713	0.755	0.31	1.760	1.04	0.429	0.585	0.14	1.250	0.68	0.468
440	0.296	0.02	0.479	0.015	0.618	0.496	0.22	1.469	0.95	0.338	0.376	0.10	1.009	0.63	0.373
488	0.154	0.02	0.337	0.015	0.459	0.264	0.13	1.217	0.86	0.217	0.194	0.06	0.817	0.57	0.238
510	0.133	0.02	0.315	0.014	0.421	0.213	0.10	1.165	0.83	0.182	0.163	0.05	0.785	0.55	0.207
532	0.125	0.02	0.296	0.013	0.421	0.185	0.08	1.106	0.81	0.167	0.145	0.04	0.756	0.54	0.191
555	0.120	0.01	0.291	0.013	0.411	0.170	0.06	1.071	0.79	0.158	0.140	0.03	0.731	0.52	0.191
650	0.370	0.01	0.521	0.012	0.711	0.400	0.04	1.211	0.73	0.330	0.370	0.01	0.931	0.46	0.398
676	0.478	0.02	0.629	0.012	0.760	0.528	0.08	1.299	0.72	0.407	0.488	0.02	1.039	0.45	0.470

3 Results and discussion

3.1 Extreme values of the degree of polarization

Examples of simulation results are presented in Figures 2a and 2b in the form of polar plots of the degree of polarization of upwelling radiance just above the sea surface. Figure 2a shows the DoP for the average IOPs measured in the open waters of the Baltic Sea for a wavelength of 412 nm in the summer season, while Figure 2b depicts an analogous case for the winter season. These two plots are characterized by one of the highest values of the peak of DoP of 0.88 for summer and 0.84 for

winter. The azimuth position of the sun is 0º in all cases. Corresponding values of computed upwelling irradiance I (in units of $Wm^{-2}sr^{-1}nm^{-1}$) are shown on the plots of Figures 2c and 2d on the logarithmic scale (due to their high angular variability).
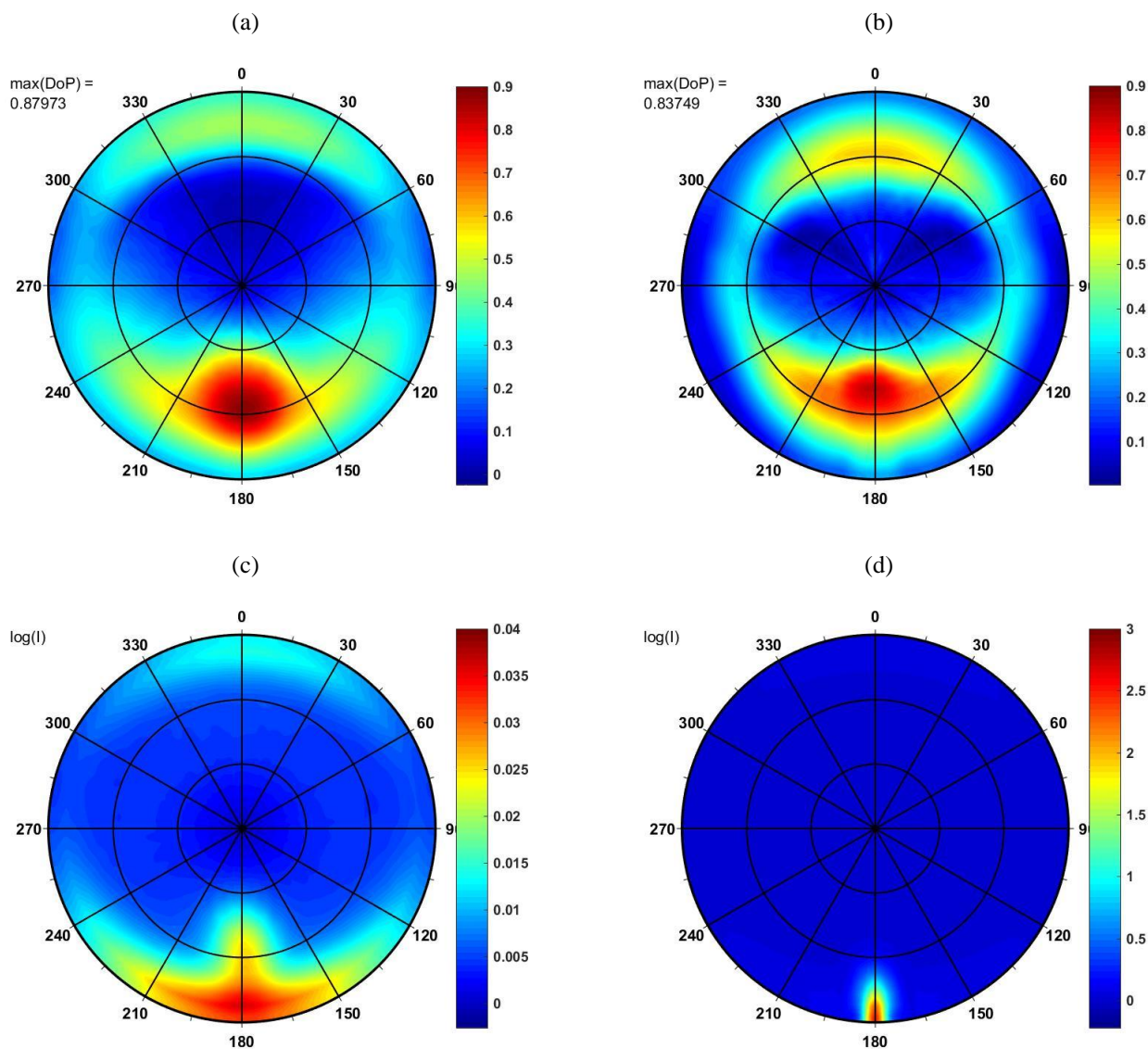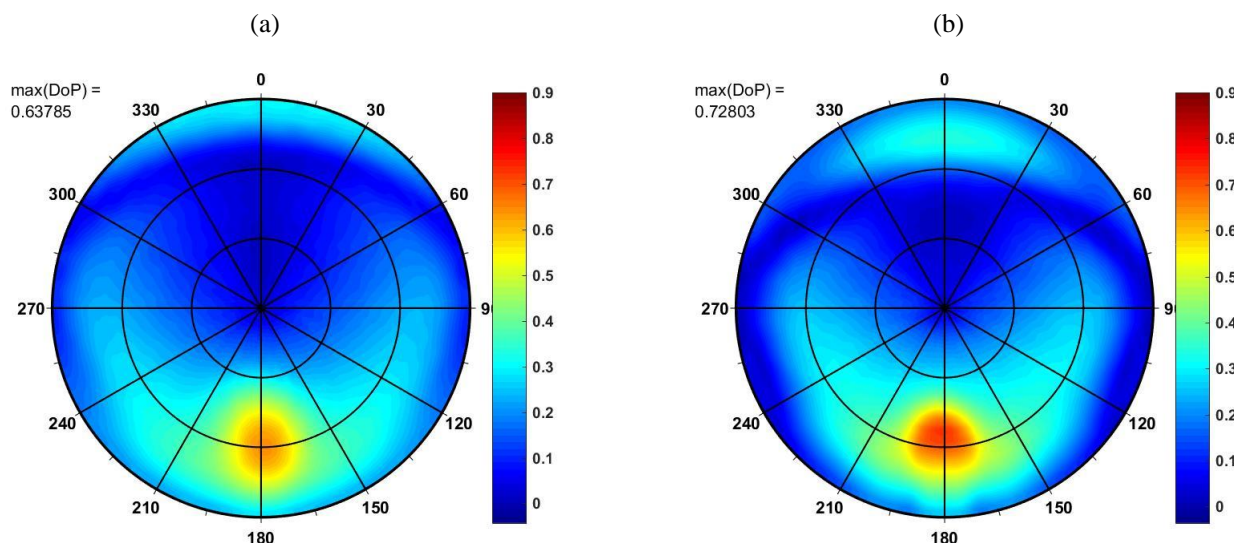

Figure 2. Simulation results of above-water upwelling radiance for average IOPs of open waters of the southern Baltic, wavelength 412 nm: a) DoP in the 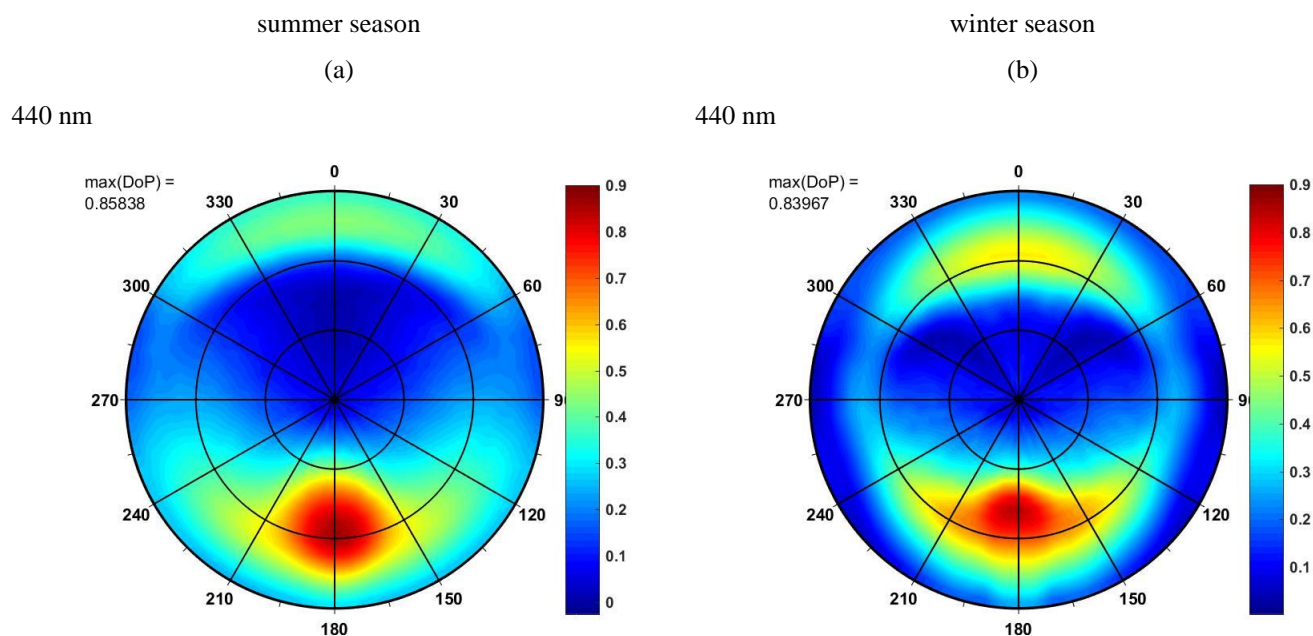summer season, SZA 45°, b) DoP in the winter season, SZA 75°, c) decimal logarithm of upwelling radiance in the summer season, SZA 45°, d) decimal logarithm of upwelling radiance in the winter season, SZA 75°.

The small SZA of the summer season (45º) resulted in low values of upwelling radiance that are stretched from the direct reflection point to the horizon, where it is extended both left and right from the azimuth of 180º. The high SZA of the winter season (75º) resulted in much higher values of reflected light, which are also stretched from reflection point to the horizon.

Ocean Science
Discussions

Examples of the lowest values of the maximum DoP, referred to as max(DoP), are shown in Figures 3a and 3b. They were

obtained for the regions of Gulf of Gdańsk and Pomeranian Gulf, simulated for the spectral band of 555 nm, for the summer

season (Figure 3a) and for the winter season (Figure 3b).

Figure 3. Simulation results of above-water upwelling radiance for average IOPs of gulf waters of the southern Baltic, wavelength 555 nm: a) DoP in the summer season, SZA 45°, b) DoP in the winter season, SZA 75°.

The maximum values of DoP presented in Figure 2a (summer season, open Baltic waters) are visible for azimuth angles

close to 180º (direction of reflected sun) and a zenith angle of approximately 55º although the solar zenith angle is 45º, while

the max(DoP) in Figure 3a (summer season, waters of gulfs) is visible for zenith angle of approximately 60º. In contrast to

the summer season case, the maximum DoPs in the winter season are close to the zenith angle of 48º (Figure 2b) and 54º

(Figure 3b), while SZA is 75º. The lower position of the sun results in a higher position of the maximum DoP of upwelling

radiation than its reflection angle, and a higher position of the sun results in a lower position of the maximum DoP. Another

interesting effect is the higher DoP observed for directions close to the incident rays of the sun (azimuth 0º). In general, in

the winter season, the values of DoP are higher than in summer, and zenith angles of this effect are lower in the winter than

in the summer season.

3.2 Spectral variability of the degree of polarization

The results of Monte Carlo simulations of angular characteristics of DoP of upwelling radiance are presented in Figure 4.

These results are obtained for average IOPs of open Baltic waters for wind speed of 5 m/s for three wavelengths (440 nm,

555 nm, 650 nm) and for both seasons. Vertical cross-sections of such polar plots for the same type of water (open Baltic

Ocean Science
Discussions

Open Access

Sea) but additionally for all examined wavelengths and for two speeds of wind, 5 m/s and 15 m/s, are presented in Figure 5. Such cross-sections show the DoP in the principal plane, including the direction of incident sun beam (on the left side of the plot), zenith and direction of sun reflection beam for calm sea surface (on the right side). The azimuth direction of the sun position, described as 0° in the polar plots, is marked by negative zenith angles in Figure 5, while azimuth directions of 180°

5 that include the sun reflection beam are marked by positive zenith angles.

summer season
(a)

440 nm

winter season
(b)

440 nm

Ocean Science
Discussions
Open Access
EGU

(c)

555 nm

(d)

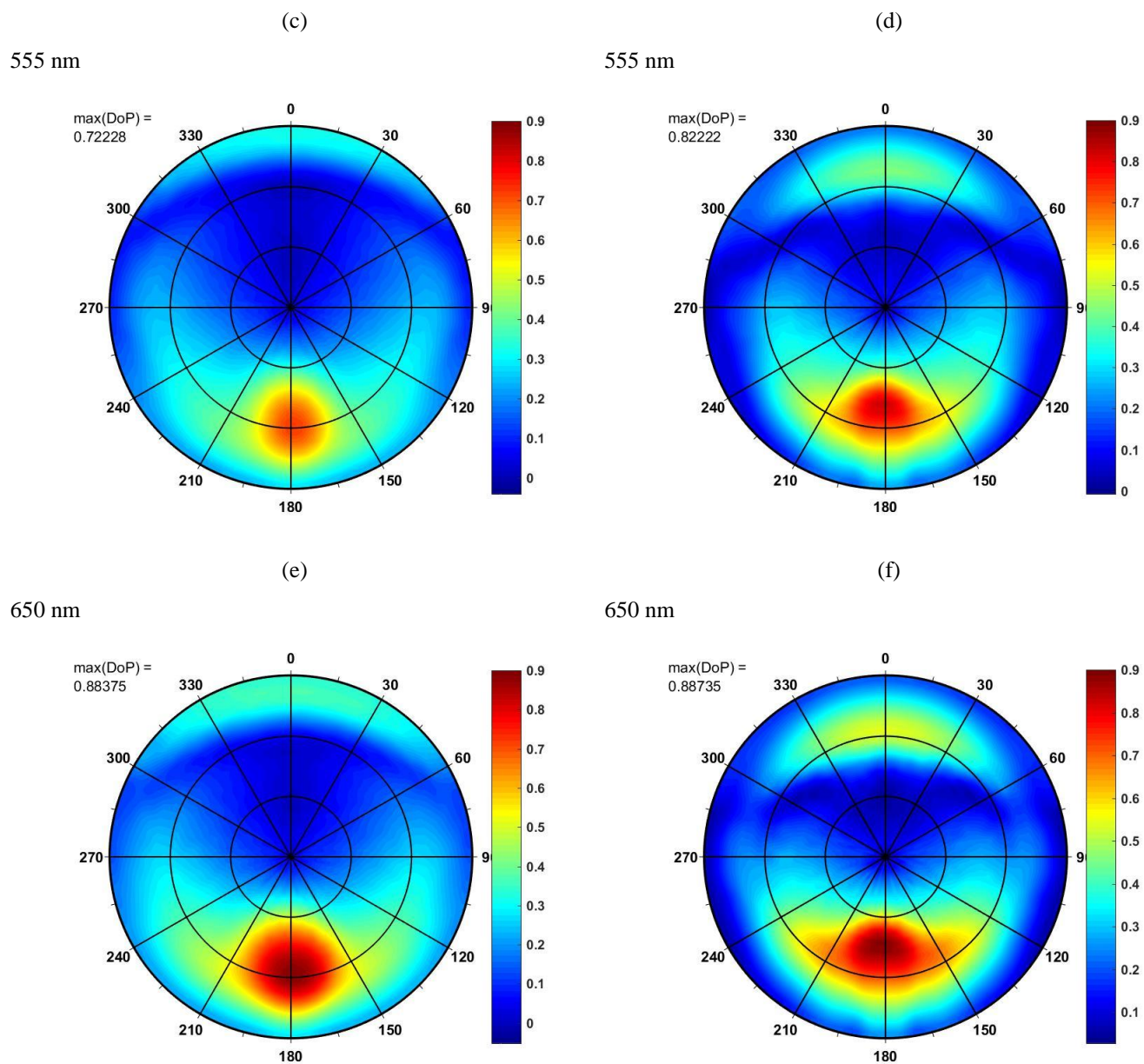555 nm

(e)

650 nm

(f)

650 nm

Figure 4. Simulation results of above-water upwelling radiance for average IOPs of open Baltic Sea water, for speed of wind of 5 m/s: a) DoP in the summer season, λ=440 nm, SZA 45°, b) DoP in the winter season, λ=440 nm, SZA 75°, c) DoP in the summer season, λ=555 nm, SZA 45°, d) DoP in the winter season, λ=555 nm, SZA 75°, e) DoP in the summer season, λ=650 nm, SZA 45°, f) DoP in the winter season, λ=650 nm, SZA 75°.

5

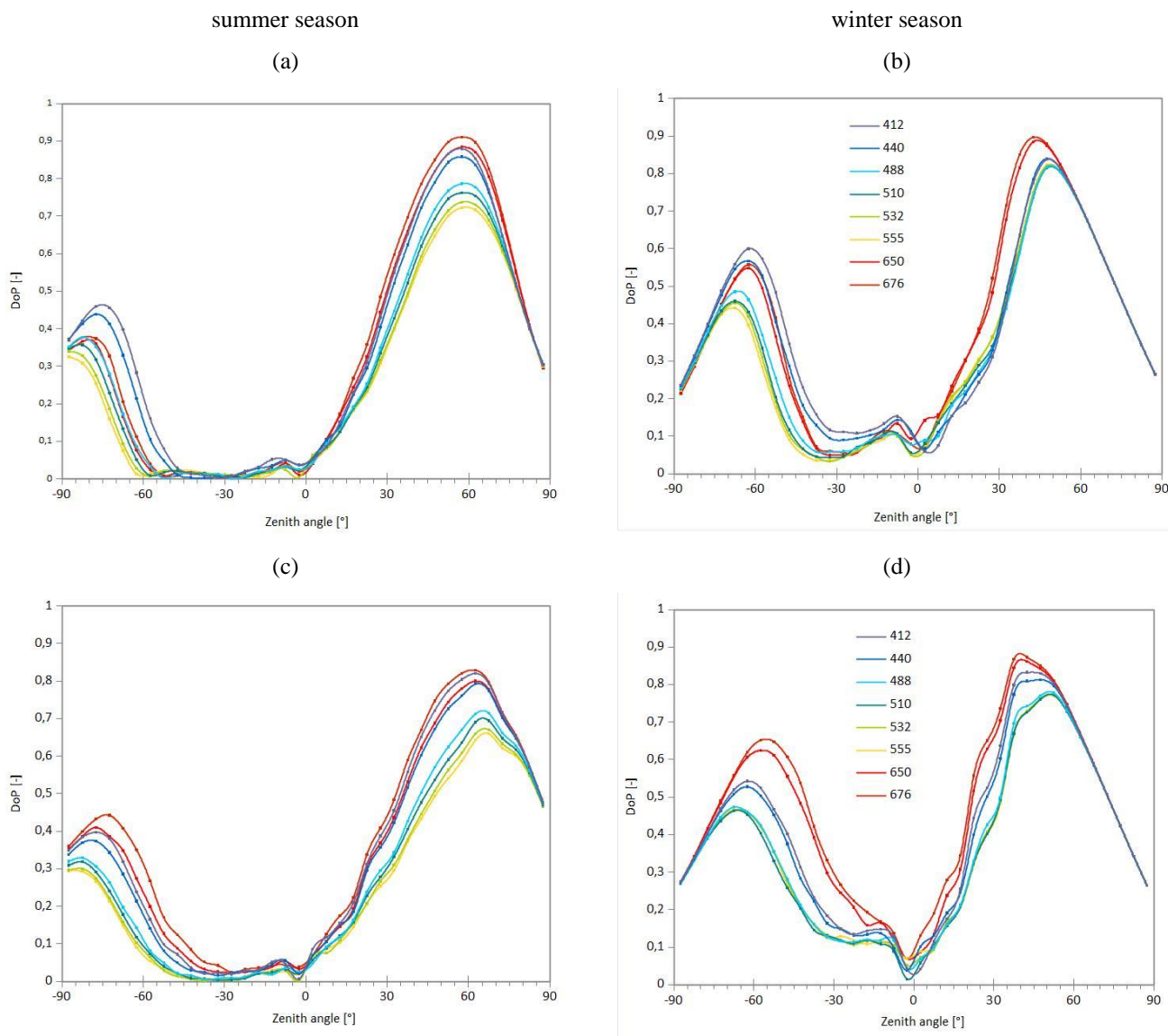summer season

winter season

(a)

(b)

(c)

(d)

Figure 5. Degree of polarization plotted for the principal plane, e.g., plane containing both incident ray of the sun and zenith direction (cross section through polar plots for azimuths 0° and 180°). Azimuth 0° - azimuth of sun position is marked by negative zenith angles, while azimuth 180° - that contains sun reflection is marked by positive zenith angles. Simulation results for open Baltic Sea water: a) summer season, SZA 45°, wind speed 5 m/s, b) winter season, SZA 75°, wind speed 5 m/s, c) summer season, SZA 45°, wind speed 15 m/s, d) winter season, SZA 75°, wind speed 15 m/s.

The analysis of individual spectral bands shows that high values of DoP correspond to the high absorption-to-attenuation ratio for the total of visible light domain (see Table 1). High values of absorption coefficient for 650-676 nm wavelengths (in the red spectral region) are caused by pure water (see Pope and Fry, 1997) while high absorption coefficients for

wavelengths of the blue-green range are caused mainly by CDOM (Kowalczuk et al., 2005). The lowest values of max(DoP) for each type of water and for each season are observed for the 555 nm spectral band. The lowest values of absorption and weak spectral variability of the scattering coefficient implies that the wavelength of 555 nm is characterized by the lowest absorption-to-attenuation ratios due to the existence of a minimum of absorption for seawater containing phytoplankton.

5   Algae cells, depending on the composition of their pigments, may have a minimum of absorption in a wide range of spectral bands from 550 nm to 660 nm (Bricaud et al., 2004). Considering the absorption of pure water that is increasing with wavelength (Pope and Fry, 1997), the minimum of the absorption in Baltic waters for the spectral band of 555 nm results.

The spectral shape of the DoP cross-sections contains two maxima, and their angular positions depend on the absorption-to-attenuation ratio, the season and the wind speed. The angular position of the higher maximum depends mostly on the season,

10   varying from approximately 60º in the summer to 35º-50º in the winter (see Figure 5). The lower maximum we observe at the zenith angles between -70º and -90º in the summer as well as between -55º and -70º in the winter. Higher wind speed of 15 m/s, in comparison to 5 m/s, causes the irregular shape of peaks. Moreover, the higher wind speed causes an increase of the DoP value for a lower maximum in the 650 nm and 676 nm spectral bands and its shift to a higher position (toward the zenith). At the same time, the DoP values for shorter wavelength bands are decreased and shifted to a lower position (toward

15   horizon).

3.3 Regional variability of the degree of polarization

Computations of DoP were carried out in three optically different regions of the southern Baltic. Such a division is justified in previous studies of optical and hydrological properties of the south Baltic waters (Olszewski et al., 1992). They showed a relationship between the measured values of IOPs and their location in relation to river estuaries, distance from the shore or

20   bathymetry of the bottom.

Comparison of water type influence on the DoP is shown in Figure 6 for two wavelengths, 440 nm (Figure 6a) and 555 nm (Figure 6b). The type of water has less influence on the DoP than the season and its representative SZA.
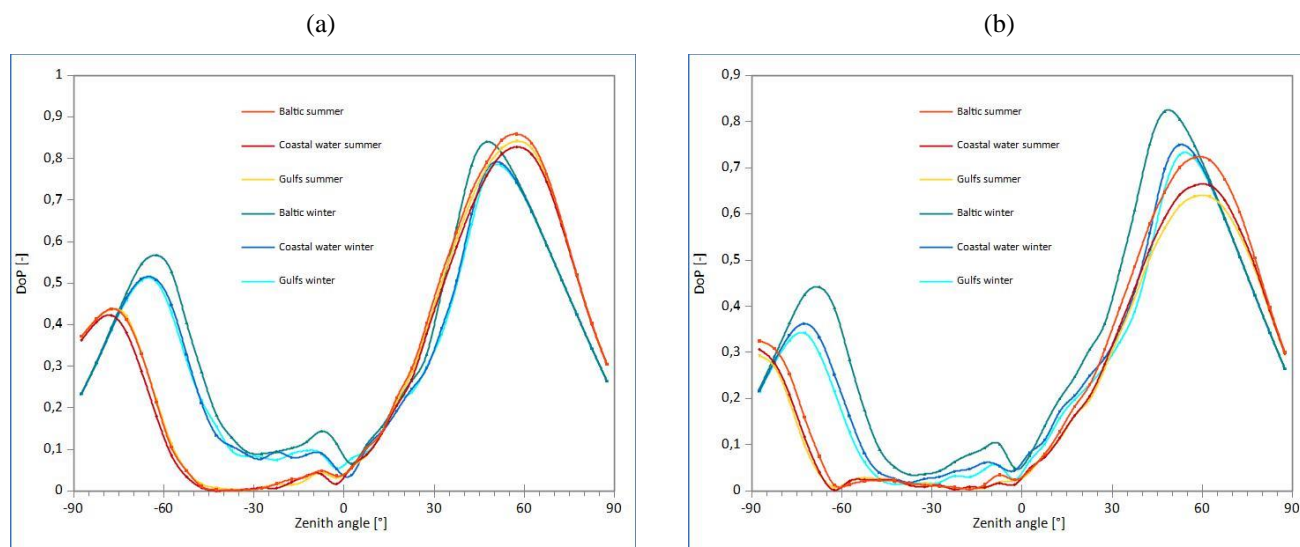
Ocean Science
Discussions

(a) (b)

Figure 6. Degree of polarization plotted for the principal plane, i.e., plane containing both incident ray of the sun and zenith direction (cross-section through polar plots for azimuths 0° and 180°). Azimuth 0° is marked by negative zenith angles. Simulation results for wind speed of 5 m/s for all types of water and two seasons: a) 440 nm, and b) 555 nm.

However, the highest values of DoP for most zenith angles and the highest values of its peak max(DoP) for each season are

5   observed for open Baltic Sea water. Coastal waters and gulfs are characterized by similar values of DoP in each season. For the wavelength of 440 nm, in the summer, the differences of max(DoP) between the open Baltic and other regions reach 0.02-0.04, while in the winter those differences exceed 0.05. For the 555 nm band, in the summer the differences of max(DoP) between the open Baltic and other regions reach 0.06-0.09 and in the winter these differences reach 0.07-0.09, respectively. We also observed another regional difference in the angular position of the maxima of DoP that is noticeable in

10   the winter season only. Two maxima of the DoP cross-sections are closer for open Baltic waters than for gulfs and coastal waters.

In the following section, we explain that the degree of polarization depends on the absorption-to-attenuation ratio, and all its regional changes are the result of the absorption-to-attenuation ratio variability.

3.4 DoP dependence on the absorption-to-attenuation ratio

15   This section contains the comparison of the degree of polarization for summer and winter seasons as a function of the absorption-to-attenuation ratio.

The total $a(\lambda)/c(\lambda)$ ratio (see Table 1) is higher in the open Baltic water than in other regions because of the low scattering coefficients (Sagan, 2008). The value of the latter is determined mainly by the concentration of suspended matter, which in open waters is significantly lower than in gulfs or coastal/near-shore waters. According to Sagan (2008), the average particle

20   scattering coefficient does not depend strongly on wavelengths, and in open Baltic waters in the winter season it varies between 0.15 (for 676 nm) and 0.19 (for 412 nm). In the same season, but in the waters of gulfs, the average particle

14

scattering coefficient varies between 0.77 (for 676 nm) and 1.00 (for 412 nm). For the influence of water type on DoP, regardless of the wavelength and wind speed, the lowest max(DoP) values in winter are observed in the waters of gulfs. These waters are characterized by the highest scattering coefficients because of the high inflow of particulate matter with river waters. However, in the summer season, the lowest peak of DoP is observed for spectral bands from 412 nm to 532 nm

5   in coastal waters, and in wavelengths from 555 nm to 676 nm in gulfs. The values of $a(\lambda)/c(\lambda)$ for these types of water differ by less than 5% except for the 650 nm and 676 nm spectral bands. According to the Fresnel equations, the reflections of two polarized components (parallel and perpendicular to the transmission/reflection plane) from the sea surface depend on two parameters only. These parameters are the relative refractive index of the medium and the angle of incidence of the light beam. Thus, polarization of the reflected light does not depend on the IOPs of seawater. The observed differences in

10   polarization of upwelling radiance above the sea surface for various absorption and attenuation coefficients of seawater come from the water-leaving component of that radiance but not from the reflected part.

All the values of maximum DoP of above-water upwelling radiance obtained for each absorption-to-attenuation ratio are collected in Figure 7. The summer season case is depicted in Figure 7a while the winter case is depicted in Figure 7b. The water types are marked with different symbols, and two wind speeds are marked with different colors. The correlations of

15   the max(DoP) to the ratio of $a(\lambda)/c(\lambda)$ are approximately linear. However, correlation coefficient analysis has shown that the power functions are better matched. The reason for the nonlinearity of this correlation may be related to the potential obtaining or even exceeding one by the value of DoP for certain combinations of absorption and attenuation coefficients. The trend line for the plot depicted in Figure 7a shows the relationship of the maximum of DoP to the ratio of $a(\lambda)/c(\lambda)$ for the summer season and in Figure 7b for the winter season, respectively. The trend lines presented may be described by

20   power functions:

$$max(DoP) = A \left(\frac{a(\lambda)}{c(\lambda)}\right)^{B},$$ (3)

whose parameters are collected in Table 2. These correlations are obtained for various spectral channels. Hence, they are wavelength-independent for the examined visible spectral range.

25   **Table 2. Parameters of equation (3), which describes the power trend lines in Figures 4 (a) and 4 (b)**

Simulation Conditions	A	B	R^2
SZA 45°, wind speed 5 m/s	1.102	0.262	0.973
SZA 45°, wind speed 15 m/s	0.997	0.250	0.996
SZA 75°, wind speed 5 m/s	0.903	0.117	0.906
SZA 75°, wind speed 15 m/s	0.914	0.173	0.990

(a)   (b)
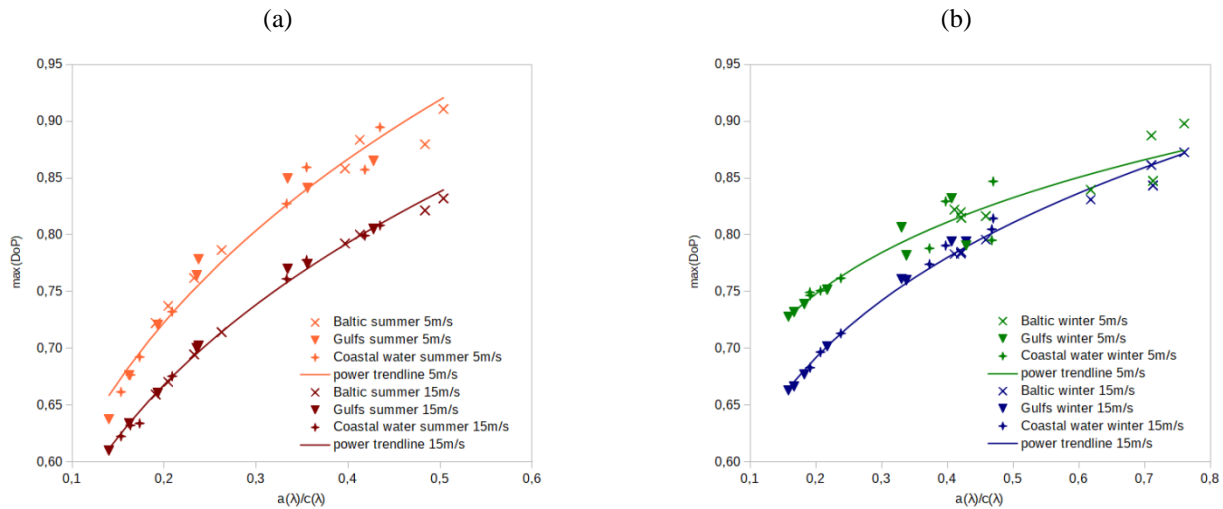

Figure 7. Values of maximum of degree of polarization against absorption to attenuation ratios a(λ)/c(λ) for average values of IOPs presented in Table 1, plotted for (a) the summer season and (b) the winter season.

An analysis of all collected data shows that higher values of maximum DoP are observed for lower wind speed. Moreover, max(DoP) has a higher range of variability in the summer season than in the winter. Figure 7a (summer season) shows that

5   values of max(DoP) are between 0.64 and 0.91 for the wind speed of 5 m/s, and between 0.61 and 0.83 for the wind speed of 15 m/s. However, in Figure 7b (winter season), the values are between 0.73 and 0.9 for the wind speed of 5 m/s, and between 0.66 and 0.87 for the wind speed of 15 m/s. Power trend lines for the same wind speed for summer and winter seasons (in Figures 7a and 7b) intersect. For a wind speed of 5 m/s, by a(λ)/c(λ) equal to 0.26, both power functions reach the same max(DoP) of 0.77. For a wind speed of 15 m/s, by a(λ)/c(λ) equal to 0.32, both power functions reach the same value of

10   0.75. For lower absorption-to-attenuation ratios, winter DoPs have higher values than summer and for higher a(λ)/c(λ) values, the summer DoPs are higher.

The reason for the correlation of the maximum DoP with the absorption-to-attenuation ratio is the occurrence of multiple scattering in water depth. The degree of polarization decreases after each act of scattering on particle matter. A high absorption-to-attenuation ratio means simply low scattering-to-attenuation impact and, hence, shallow penetration of light in

15   the water column and low participation in multiple scattering that decreases the DoP. Such conclusion is in accordance with Piskozub and Freda (2013), who examined the influence of single scattering albedo on the polarization of water-leaving radiance. Their results show that in the sun reflection plane, the highest value of DoP is observed when the total scattering coefficient is the lowest (see Figure 3 in Piskozub and Freda (2013)).

The influence of wind speed on the DoP values shown in Figures 7a and 7b is very clear: sea surface roughness depolarizes

20   the reflected light. Zhou et al. (2013) demonstrated that wind speed and wind direction can change the polarization patterns of reflected skylight from a rough sea surface to a certain extent. Our study shows, in particular, that high wind speed results in lower values of max(DoP) of the total upwelling radiance. Such regularity is filled for all types of water and all spectral bands.

Ocean Science
Discussions

Open Access

EGU

3.5 Direction of the highest polarization peak

Moreover, as an attempt to explain the differences between seasons, the DoPs of underwater upwelling radiances were simulated. The results of the computations are shown in Figures 8a and 8b, and the corresponding values of the radiance

5 field are presented in Figures 8c and 8d. These plots indicate that directions characterized by high values of DoP create a dispersed ring, which is tilted from the horizontal direction. The angular tilt of the ring plane is approximately 60º for the summer season and 45º for the winter. Moreover, both the underwater upwelling spectral radiance and its DoP are higher in the summer season than in the winter season.

a)   (b)
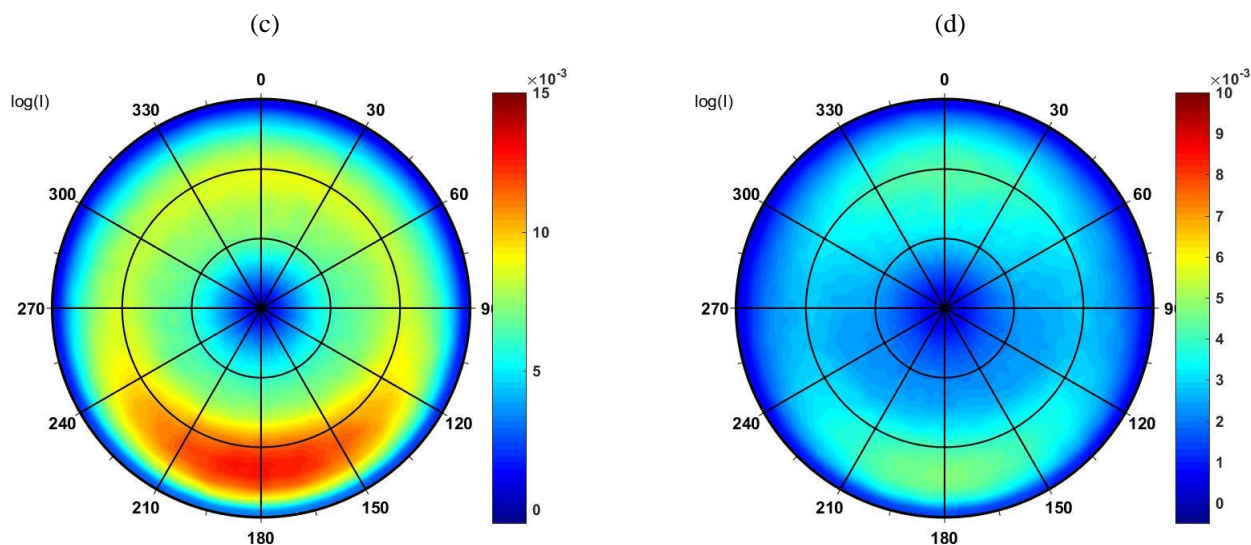
Ocean Science
Discussions

Open Access

(c)

(d)
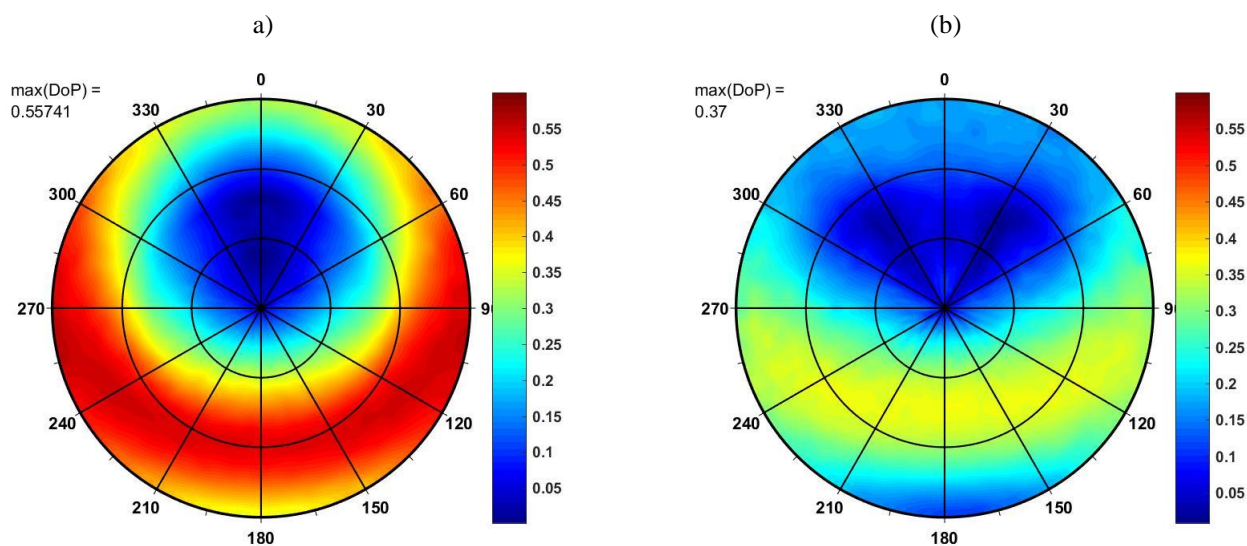
Figure 8. Simulation results of underwater upwelling radiance for average IOPs of open waters of the southern Baltic, wavelength 412 nm: a) DoP in the summer season, SZA 45°, b) DoP in the winter season, SZA 75°, c) decimal logarithm of upwelling radiance in the summer season, SZA 45°, d) decimal logarithm of upwelling radiance in the winter season, SZA 75°.

5

The angular position of highly polarized radiance for both below and above the sea surface is schematically shown in Figure 9. For a plane including sun reflection and refraction (azimuth 0° and 180°) if the surface is calm, then for the SZA of 45°, the transmission angle TA, according to Snell's law, is 32°. Underwater polarization, caused by molecular scattering, is the highest in the plane perpendicular to the direction of propagation. In the vertical plane including transmitted rays, the highest
10 polarization of molecular scattering (HPM) is 58°. For SZA of 75°, the transmission angle is 46° and direction of HPM is 44°. Directions of HPM predicted for a calm sea surface proved to be the same for a wind-roughened sea surface (see the polarization patterns in Figures 2a and 2b). The angular position of HPM, which is perpendicular to TA in the reflection-refraction plane, is both predicted by theory (molecular scattering) and confirmed by the underwater measurements of Tonizzo et al. (2009). Their underwater DoPs, measured in waters characterized by various optical properties and a depth of
15 one meter, slightly exceed the value of 0.4 by the detection angle close to 100° (see their Figure 9), while our simulated underwater values of DoP reach even 0.55 (Figure 8a). The difference may be because the measurements of Tonizzo et al. were performed at a depth of 1 m, and our simulation is obtained for depths just below 0 m.
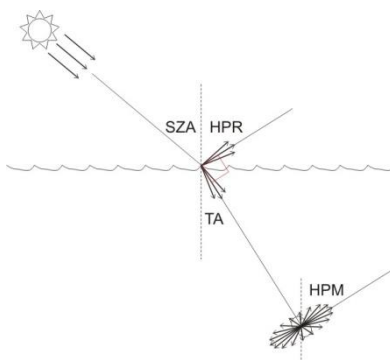
Figure 9. Diagram of directions of High Polarization radiance for surface Reflections (HPR) and High Polarization for Molecular scattering (HPM)

5   The highest polarization of reflected radiance (HPR), according to Fresnel equations for a flat reflective surface, should appear when the reflection angle is perpendicular to TA. Figures 2a and 2b show that for a rough sea surface, the HPR direction is not equal to the angle of incidence (SZA). For SZA of 45º (summer season case), the HPR is dispersed approximately 56º (see Figure 2a) while for a calm surface it would be exactly 58º. Moreover, the sum of SZA and zenith angle of HPR is 101º, which is very close to double the Brewster angle, that for water is approximately 53º. That could

10 explain the angular position of HPR. However, for SZA of 75º (representing the winter season in the southern Baltic), the HPR is dispersed around the zenith angle of 48º (see Figure 2b). Here, the direction perpendicular to TA is 44º (see Figure 8b). The sum of SZA and HPR is 123º, which is much higher than double the Brewster angle. For this reason, the position of the HPR for rough sea surface should be interpreted rather as the direction perpendicular to the average TA, than the reflection from these surface slopes for which the angles of incidence and reflection are both equal to the Brewster angle.

15

The unpolarized sunlight after reflection or refraction processes at the sea surface becomes partly polarized. As an attempt to explain high differences between values of upwelling radiance over sea surface shown in the Figures 2c and 2d, we applied Fresnel equations to calculate both the transmission and reflection fractions of two polarization components of that light, namely, the parallel and the perpendicular. These fractions depend strongly on the solar zenith angle of incident light. For a

20 calm surface, SZA of 45º (corresponding to the summer season) and TA of 32º, only 0.3% of the parallel polarized light component is reflected by the surface, and 99.7% is transmitted to the water depth, while for the perpendicular polarized part much more (5.5%) is reflected and 94.5% is transmitted through the surface. For an SZA of 75º (winter season) and a TA of 46°, the reflected fraction would be 11% for the parallel polarization component and as much as 32% for the perpendicular component, while the transmission would be equal to 89% and 68%, respectively (see Table 3). These calculations show that

25 for SZA of 45º the reflected part of the upwelling radiance is much lower than for an SZA of 75º, and the contribution of the perpendicular component of polarization is much higher than the parallel, resulting in a higher degree of polarization of the

Ocean Science
Discussions

reflected part of the total upwelling radiance in the summer season because of higher disproportion of one polarization component.

Table 3. The contribution to the processes of reflection and transmission through flat sea surface, calculated according to Fresnel
5 **equations for two polarization components of unpolarized light coming from SZA. These polarization components are perpendicular and parallel to the plane of reflection-refraction.**

Summer Season, SZA = 45°			
Parallel		Perpendicular	
Reflection	Transmission	Reflection	Transmission
0.3%	99.7%	5.5%	94.5%
Winter Season, SZA = 75°			
Parallel		Perpendicular	
Reflection	Transmission	Reflection	Transmission
11%	89%	32%	68%

Polarization patterns of total upwelling radiance, combined with radiance reflected off the sea surface and water-leaving radiance, differ from those describing only the reflected part obtained by Zhou et al. (2013). As the reflected part of the
10 upwelling radiance forms 90% and more of the total upwelling radiance during sunny days, the contribution of water-leaving radiance to the polarization changes is detectable. Zhou et al. (2013) show that the DoP of the reflected radiance component creates a ring of high values at the polar plot called the Brewster zone. The angular shape of this zone depends strongly on the SZA (see Figure 10 in Zhou et al. (2013)) and the polarization direction in this area is almost perpendicular to the local meridian. In our study, low transmission of light into the water depth in the winter case (SZA of 75º) in comparison to the
15 summer case (SZA of 45º) also explains the differences in underwater upwelling radiances (see Figures 8c and 8d). Underwater radiance and its polarization have a higher influence on polarization of upwelling radiance over the sea surface in the summer than in the winter. Lower SZA causes higher transmission into the water depths and higher scattering toward the sea surface, so DoP distribution of upwelling radiance in winter looks more similar to a polarization pattern of the reflected part presented by Zhou et al. (2013) with their ring-shaped Brewster zone.
20 The results of our simulations are in qualitative agreement with the measurements of above water DoLP of the total upwelling radiance presented by Freda et al. (2015). This agreement is the similarity of the peak of degree of polarization on the polar plots, which are stretched along the azimuth angles. Freda et al. (2015) obtained lower values of measured DoLP with a maximum of 30-40% (see Figures 1 and 2 in (Freda et al., 2015)), which is presumably caused by different weather conditions and unknown environmental parameters during measurements, such as a high absorption coefficient in the waters
25 of the river mouth, different aerosol optical depth, or other parameters. However, despite the differences in the maximum

degree of polarization, the angular distribution patterns are similar, with the peak in the vicinity of the sun reflection azimuth angle.

The results of the correlation of the maximum DoP with the absorption-to-attenuation ratio seem to be coincident with the results of Ibrahim et al., (2012) who studied the degree of linear polarization just below the air-water interface. Their

5   correlation of attenuation-to-absorption ratio with DoLP displays a hyperbolic-like shape (see Figures 5 to 8 in Ibrahim et al. 2012). Therefore, for an inverted ratio of absorption-to-attenuation, it would be near-linear. The modeling results of Ibrahim et al. cannot be compared directly to the results presented in this paper because they received DoLP just below the sea surface, and we focused on DoP just above the surface. However, our choice of seawater absorption-to-attenuation ratio, which can be called the relative absorption value (to total attenuation), as a parameter correlated to degree of polarization

10   seems to be more suitable.

5 Conclusions

In this paper, we have investigated the relationship between the seawater absorption-to-attenuation ratio and the degree of radiance polarization above the rough sea surface. Using a Monte Carlo polarized radiative transfer model, we compared/analyzed simulated polarization patterns in three optically different regions in the southern Baltic (i.e., open

15   Baltic, gulfs, coastal waters), two seasons (defined by their typical solar zenith angles: 45º for summer and 75º for winter), and two wind speeds of 5 m/s and 15 m/s, each for nine visible spectral bands (412 nm, 440 nm, 488 nm, 510 nm, 532 nm, 555 nm, 650 nm, 676 nm, 715 nm). The use of the modeling tool allowed us to exclude unwanted and unpredictable variables (such as weather conditions and aerosol optical thickness) and to conduct undisturbed comparison of the DoPs of combined water-leaving and reflected components of upwelling radiance.

20   We found that the variability of the maximum of DoP depends more on seasonal than regional changes and can be explained to a large degree by the absorption-to-attenuation ratio. A thorough analysis has shown that there is a strong correlation between max(DoP) and the ratio mentioned previously. The correlation is well described ($R^2 > 0.90$) by a power function with factor A close to one and factor B depending more on SZA than on the wind speed. In our study, seasonal variability of the degree of polarization is higher/more significant than regional variability. However, this may be true only in the southern

25   Baltic region due to the characteristically different SZA ranges in the winter and summer seasons.

Further supplementary simulations of underwater polarization distribution have shown that the directions of max(DoP) of combined water-leaving and reflected components of upwelling radiance are dispersed in directions perpendicular to the undersurface transmission angle.

For the ocean color remote sensing application, only the water-leaving part of the upwelling radiance carries useful

30   information about bio-optical parameters of seawater, although it is a small fraction of the total upwelling radiance. Polarized radiative transfer modeling makes it possible to separate the water-leaving part and, in this case, noise-inducing reflected part and therefore to enhance the quality of information on the seawater optically active components retrieved by

Ocean Science

Discussions

Open Access

EGU

above-water sensors – airborne or satellites. Our study is a step toward inclusion of polarization properties in the bio-optical models in the Baltic Sea. However, the conclusions from the research, in our opinion, should be universal and apply also to other water bodies.

References

Benassai, G., Montuori, A., Migliaccio, M., and Nunziata, F.: Sea wave modeling with X-band COSMO-SkyMed© SAR-
10 derived wind field forcing and applications in coastal vulnerability assessment, Ocean Sci., 9, 325-341, doi:10.5194/os-9-325-2013, 2013.

Berthon, J. F., Shybanov, E., Lee, M., and Zibordi, G.: Measurements and modeling of the volume scattering function in the coastal northern Adriatic Sea, Appl. Opt., 46, 5189-5203, doi:10.1364/AO.46.005189, 2007.

Bricaud, A., Claustre, H., Ras, J., and Oubelkheir K.: Natural variability of phytoplanktonic absorption in oceanic waters:
15 Influence of the size structure of algal populations, J. Geophys. Res., 109, C11010, doi:10.1029/2004JC002419, 2004.

Chami, M.: Importance of the polarization in the retrieval of oceanic constituents from the remote sensing reflectance. J. Geophys. Res., 112, C05026, doi:10.1029/2006JC003843, 2007.

Chami, M., Shybanov, E. B., Churilova, T. Y., Khomenko, G. A., Lee, M. E.-G., Martynov, O. V., Berseneva, G. A., and Korotaev, G. K.: Optical properties of the particles in the Crimea coastal waters (Black Sea), J. Geophys. Res. 110, C11020,
20 doi:10.1029/2005JC003008, 2005.

Chowdhary, J., Cairns, B., and Travis, L. D.: Case studies of aerosol retrievals over the ocean from multiangle, multispectral photopolarimetric remote sensing data, J. Atmos. Sci. 59, 383-397, doi:10.1175/1520-0469(2002)059<0383:CSOARO>2.0.CO;2, 2002.

Cox, C., and Munk, W.: Slopes of the Sea Surface Deduced from Photographs of Sun Glitter; Bulletin of the Scripps
25 Institution of Oceanography of the University of California, La Jolla; University of California Press: Oakland, CA, USA, 1956.

Cunningham, A., Wood, P., and McKee D.: Brewster-angle measurements of sea-surface reflectance using a high resolution spectroradiometer, J. Opt. A: Pure Appl. Opt., 4, S29-S33, doi:10.1088/1464-4258/4/4/361, 2002.

Drozdowska, V., Wróbel, I., Markuszewski, P., Makuch, P., Raczkowska, A., and Kowalczuk, P.: Study on organic matter
30 fractions in the surface microlayer in the Baltic Sea by spectrophotometric and spectrofluorometric methods, Ocean Sci., 13, 633-647, https://doi.org/10.5194/os-13-633-2017, 2017.

Freda, W.: Comparison of the spectral-angular properties of light scattered in the Baltic Sea and oil emulsions, J. Europ. Opt. Soc. Rap. Public., 9, 14017, doi:10.2971/jeos.2014.14017, 2014.

Freda, W.: Spectral dependence of the correlation between the backscattering coefficient and the volume scattering function measured in the Southern Baltic Sea, Oceanologia, 54, 355-367, doi:10.5697/oc.54-3.355, 2012.

5   Freda, W., Król, T., Martynov, O. V., Shybanov, E. B., and Hapter, R., Measurements of scattering function of sea water in southern Baltic, Eur. Phys. J. Special Topics, 144, 147-154, doi:10.1140/epjst/e2007-00119-6, 2007.

Freda, W., and Piskozub, J.: Improved method of Fournier-Forand marine phase function parameterization, Opt. Express, 15, 12763-12768, doi:10.1364/OE.15.012763, 2007.

Freda, W., Piskozub, J., and Toczek H.: Polarization imaging over sea surface - a method for measurements of Stokes

10   components angular distribution, J. Europ. Opt. Soc. Rap. Public. 10, 15060, doi:10.2971/jeos.2015.15060, 2015.

Frouin, R., Pouliquen, E., Breon, F.-M.: Ocean color remote sensing using polarization properties of reflected sunlight, in:, CNES, Proceedings of 6th International Symposium on Physical Measurements and Signatures in Remote Sensing, Val D'Isere, France, 17-22 January 1994, 665-674, 1994.

Garaba, S., and Zielinski, O.: Methods in reducing surface reflected glint for shipborne above-water remote sensing, J.

15   Europ. Opt. Soc. Rap. Public., 8, 13058, doi:10.2971/jeos.2013.13058, 2013.

Gilerson, A., Zhou, J., Oo, M., Chowdhary, J., Gross, B. M., Moshary, F., and Ahmedet, S.: Retrieval of chlorophyll fluorescences from reflectance spectra through polarization discrimination: modeling and experiments, Appl. Opt. 45, 5568-5581, doi:10.1364/AO.45.005568, 2006.

Hajnsek, I., Pottier, E., and Cloude, S. R.: Inversion of surface parameters from polarimetric SAR, IEEE Transactions on

20   Geoscience and Remote Sensing, vol. 41, 4, 727-744, doi:10.1109/TGRS.2003.810702, 2003.

Harmel, T., and Chami, M.: Influence of Polarimetric Satellite Data Measured in the Visible Region on Aerosol Detection and on the Performance of Atmospheric Correction Procedure over Open Ocean Waters. Opt. Express, 19, 20960-20983, doi:10.1364/OE.19.020960, 2008.

Hasekamp, O. P., and Landgraf, J.: Retrieval of aerosol properties over the ocean from multispectral single-viewing-angle

25   measurements of intensity and polarization: Retrieval approach, information content, and sensitivity study, J. Geophys. Res. 110, doi:10.1029/2005JD006212, 2005.

Haule, K., and Freda W.: The effect of dispersed Petrobaltic oil droplet size on photosynthetically active radiation in marine environment, Environ. Sci. Pollut. Res., 23, 6506-6516, doi:10.1007/s11356-015-5886-4, 2016.

Haule, K., Freda, W., Darecki, M., and Toczek, H.: Possibilities of optical remote sensing of dispersed oil in coastal waters,

30   Estuarine, Coastal and Shelf Science, 195, 76-87, doi:10.1016/j.ecss.2016.07.013, 2017.

He, X., Pan, D., Bai, Y., Wang, D., and Hao, Z.: A new simple concept for ocean colour remote sensing using parallel polarisation radiance, Scientific Reports, 4, 3748, doi:10.1038/srep03748, 2014.

Ibrahim, A., Gilerson, A., Harmel, T., Tonizzo, A., Chowdhary, J., and Ahmed, S.: The relationship between upwelling underwater polarization and attenuation/absorption ratio. Opt. Express 23, 25662-25680, doi:10.1364/OE.20.025662, 2012.

Kowalczuk, P.: Seasonal variability of yellow substances absorption in the surface layer of the Baltic Sea, J. Geophys. Res., 104, 30047-30058, doi:10.1029/1999JC900198, 1999.

Kowalczuk, P. and Kaczmarek, S.: Analysis of temporal and spatial variability of "yellow substance" absorption in the Southern Baltic, Oceanologia, 38, 3-32, 1996.

5   Kowalczuk, P., Olszewski, J., Darecki, M., and Kaczmarek, S.: Empirical relationships between coloured dissolved organic matter (CDOM) absorption and apparent optical properties in Baltic Sea waters, Int. J. Remote Sens., 26, 345-370, doi:10.1080/01431160410001720270, 2005.

Kowalczuk, P., Stedmon, C. A., and Markager, S.: Modeling absorption by CDOM In the Baltic Sea from season, salinity and chlorophyll, Mar. Chem., 101, 1-11, doi:10.1016/j.marchem.2005.12.005, 2006.

10 Kowalczuk, P., Darecki, M., Zabłocka, M., and Górecka, I.: Validation of empirical and semi-analytical remote sensing algorithms for estimating absorption by Coloured Dissolved Organic Matter in the Baltic Sea from SeaWiFS and MODIS imagery, Oceanologia, 52, 171-196, doi:10.5697/oc.52-2.171, 2010.

Lee M. E., and Lewis, M. R.: A new method for the measurement of the optical volume scattering function in the upper ocean, J. Atmos. Ocean. Technol., 20, 563-571, 2003.

15 Liu, J., He, X., Liu, J., Bai, Y., Wang, D., Chen, T., Wang, Y., and Zhu, F.: Polarization-based enhancement of ocean color signal for estimating suspended particulate matter: radiative transfer simulations and laboratory measurements, Opt. Express 25, A323-A337, doi:10.1364/OE.25.00A323, 2017.

Loisel, H., Duforet, L., Dessailly, D., Chami, M., and Dubuisson, P.: Investigation of the Variations in the Water Leaving Polarized Reflectance from the POLDER Satellite Data over two Biogeochemical Contrasted Oceanic Areas. Opt. Express;

20 16, 12905-12918, doi:10.1364/OE.16.012905, 2008.

Meler, J., Kowalczuk, P., Ostrowska, M., Ficek, D., Zabłocka, M., and Zdun, A.: Parameterization of the light absorption properties of chromophoric dissolved organic matter in the Baltic Sea and Pomeranian lakes, Ocean Sci., 12, 1013-1032, doi:10.5194/os-12-1013-2016, 2016a.

Meler, J., Ostrowska, M., and Stoń-Egiert, J.: Seasonal and spatial variability of phytoplankton and non-algal absorption in

25 the surface layer of the Baltic, Estuarine, Coastal and Shelf Science, 180, 123-135, doi:10.1016/j.ecss.2016.06.012, 2016b.

Mishchenko, M. I., and Travis, L. D.: Satellite retrieval of aerosol properties over the ocean using polarization as well as intensity of reflected sunlight, J. Geophys. Res. 102, 16989-17013, doi:10.1029/96JD02425, 1997.

Olszewski J., Sagan S., and Darecki M.: Spatial and temporal changes in some optical parameters in the southern Baltic, Oceanologia, 33, 87-103, 1992.

30 Otremba Z., Zielinski, O., and Hu, C.: Optical contrast of oil dispersed in seawater under windy conditions, Journal of the European Optical Society - Rapid Publications, 8, 13051, doi:10.2971/jeos.2013.13051, 2013.

Otremba, Z.: Oil Droplet clouds suspended in the sea: can they be remotely detected?, Remote Sens., 8, 857, doi:10.3390/rs8100857, 2016.

Piskozub J., and Freda. W.: Signal of single scattering albedo in water leaving polarization, Journal of the European Optical Society – Rapid Publications, 8, 13055, doi:10.2971/jeos.2013.13055, 2013.

Pope, R. M. and Fry, E. S.: Absorption spectrum (380-700 nm) of pure water. II Integrating cavity measurements, Appl. Optics, 36, 8710-8723, doi:10.1364/AO.36.008710, 1997.

5 Pust, N. J., Dahlberg, A. R., Thomas, M. J., and Shaw, J. A.: Comparison of full-sky polarization and radiance observations to radiative transfer simulations which employ AERONET products, Opt. Express, 19, 18602-18613, doi:10.1364/OE.19.018602, 2011.

Rudź, K., Darecki, M. and Toczek, H.: Modelling the influence of oil content on optical properties of seawater in the Baltic Sea. J. Europ. Opt. Soc. Rap. Public. 8, 13063, doi:10.2971/jeos.2013.13063, 2013.

10 Sagan, S.: The inherent water optical properties of Baltic waters (in Polish), Diss. Monogr., 21, IOPAS Sopot, Poland, pp. 244, 2008.

Sammartino, M., Di Cicco, A., Marullo, S., and Santoleri, R.: Spatio-temporal variability of micro-, nano- and pico-phytoplankton in the Mediterranean Sea from satellite ocean colour data of SeaWiFS, Ocean Sci., 11, 759-778, doi: 10.5194/os-11-759-2015, 2015.

15 Siegel, D. A., Wang, M., Maritorena, S., and Robinson, W.: Atmospheric correction of satellite ocean color imagery: the black pixel assumption, Appl. Opt. 39, 3582-3591, doi:10.1364/AO.39.003582, 2000.

Smith, R., and Baker, K.: Optical properties of the clearest natural waters (200-800 nm), Appl. Opt. 20, 177-184, doi:10.1364/AO.20.000177, 1981.

Soloviev, A., Maingot, C., Matt, S., Dodge, R. E., Lehner, S., Velotto, D., Brusch, S., Perrie, W., and Hochberg, E.: Fine-
20 scale features on the sea surface in SAR satellite imagery – Part 1: Simultaneous in-situ measurements, Ocean Sci. Discuss., 9, 2885-2914, doi: 10.5194/osd-9-2885-2012, 2012.

Tonizzo, A., Gilerson, A., Harmel, T., Ibrahim, A., Chowdhary, J., Gross, B., Moshary, F., and Ahmed S.: Estimating particle composition and size distribution from polarized water-leaving radiance. Appl. Opt. 50, 5047-5058, doi:10.1364/AO.50.005047, 2011.

25 Tonizzo, A., Zhou, J., Gilerson, A., Twardowski, M. S., Gray, D. J., Arnone, R. A., Gross, B. M., Moshary, F., and Ahmed, S. A.: Polarized light in coastal waters: hyperspectral and multiangular analysis, Opt. Express, 17, 5666-5683 doi:10.1364/OE.17.005666, 2009.

Volpe, G., Colella, S., Forneris, V., Tronconi, C., and Santoleri, R.: The Mediterranean Ocean Colour Observing System – system development and product validation, Ocean Sci., 8, 869-883, doi:10.5194/os-8-869-2012, 2012.

30 Volten, H., Muñoz, O., Rol, E., de Haan, J. F., Vassen, W., Hovenier, J., Muinonen, K., Nousiainen T.: Scattering matrices of mineral aerosol particles at 441.6 nm and 632.8 nm, Journal of Geophysical Research, 106, 17375-17401, doi:10,1029/2001JD900068, 2001.

Voss, K. J., and Fry, E. S.: Measurement of the Mueller matrix for ocean water, Appl. Opt. 23, 4427-4439, doi:10.1364/AO.23.004427, 1984.

Ocean Science
Discussions

Open Access

EGU

Wang, M.: Remote sensing of the ocean contributions from ultraviolet to near-infrared using the shortwave infrared bands: simulations, Appl. Opt. 46, 1535-1547, doi:10.1364/AO.46.001535, 2007.

Wood, P., and Cunningham, A.: Ship-borne measurements of ocean colour: Development of a CCD-based reflectance radiometer and trials on a longitudinal transect of the Atlantic Ocean, International Journal of Remote Sensing, 22, 99-111,

5   doi:10.1080/014311601750038875, 2001.

Woźniak, S. B., Meler, J., Lednicka, B., Zdun, A., and Stoń-Egiert, J.: Inherent optical properties of suspended particulate matter in the southern Baltic Sea, Oceanologia, 53, 691-729, doi:10.5697/oc.53-3.691, 2011.

Zaneveld J. R. V., Kitchen, J. C., and Moore, C.: The scattering error correction of reflecting tube absorption meters, Proc. SPIE, 2258, 44–55, doi: 10.1117/12.190095, 1994.

10   Zhai, P., Knobelspiesse, K., Ibrahim, A., Franz, B., Hu, Y., Gao, M., and Frouin, R.: Water-leaving contribution to polarized radiation field over ocean, Opt. Express 25, A689-A708, doi:10.1364/OE.25.00A689, 2017.

Zhou, G., Xu, W., Niu, C., and Zhao, H.: The polarization patterns of skylight reflected off wave water surface, Opt. Express 21, 32549-32565,doi:10.1364/OE.21.032549, 2013.

Zhou, G., Xu, W., Niu, C., Zhang, K., Ma, Z., Wang, J., and Zhang,Y.: Versatile time-dependent spatial distribution model

15   of sun glint for satellite-based ocean imaging, J. Appl. Rem. Sens., 11, 016020, doi:10.1117/1.JRS.11.016020, 2017.

Zibordi, G., Mélin, F., Berthon, J.-F., and Canuti, E.: Assessment of MERIS ocean color data products for European seas, Ocean Sci., 9, 521-533, doi:10.5194/os-9-521-2013, 2013.